Aerostructural Optimization of Drooped Wings

Shahriar Khosravi* and David W. Zingg†

Institute for Aerospace Studies, University of Toronto

4925 Dufferin Street, Toronto, Ontario, M3H 5T6, Canada

Through aerostructural optimization, this paper presents progress towards characterizing the potential efficiency gains of drooped wings for commercial aircraft in transonic flight. The drooped wing is a nonplanar configuration with downward spanwise camber from the wing root to the tip. The aerostructural optimization cases include two load conditions: cruise and $2.5g$. The single $2.5g$ maneuver load condition is used for structural sizing of the wing. In all cases, the projected span of the wing remains unchanged. The results show that such a wing has the potential to improve aircraft range by 2.6% relative to an optimized planar wing of the same projected span. The reason is that the drooped wing pushes the tip vortex further away than the planar wing and increases the projected span at the deflected state. Furthermore, if the drooped wing is permitted to have curved leading and trailing edges, a 4.9% range improvement in comparison to an optimized planar wing with straight leading and trailing edges is possible by further reducing wing weight and wave drag.

*Ph.D. Graduate, Corresponding Author, shahriar.khosravi@mail.utoronto.ca

†Distinguished Professor of Computational Aerodynamics and Sustainable Aviation, Institute for Aerospace Studies, Director, Centre for Research in Sustainable Aviation, Associate Fellow AIAA

Nomenclature

b	Wing span	M	Freestream Mach number
$b^\star$	Projected span under deflections	q_∞	Freestream dynamic pressure
C_L	Lift coefficient	R	Range parameter
C_p	Pressure coefficient	S_{wetted}	Wetted surface area
D	Total drag	W	Wing weight
D_{induced}	Induced drag	W_0	Wing weight of the initial design
e	Span efficiency factor	W_{fuel}	Fuel weight
g	Gravitational acceleration constant	W_{MTO}	Maximum takeoff weight
$\mathcal{J}$	Optimization objective function	x, y, z	Streamwise, spanwise, and vertical coordinates
L	Lift	ϕ	Dihedral angle

I. Introduction

Although the relative contribution of the aviation sector to overall human-induced greenhouse gas emissions is currently small, it is still a point of concern due to the fast growth of the airline industry. Airbus project that the industry will grow by an average annual rate of 4.6% in terms of revenue passenger kilometers over the next five decades [1]. However, this kind of growth in air travel without increasing harmful emissions is only possible with substantially more efficient aircraft. Modern tube-and-wing aircraft are highly optimized and offer little potential for further significant efficiency improvements. Therefore, novel design concepts must be explored.

The drooped wing is a nonplanar concept with the potential to reduce induced drag. The nonplanar nature of this configuration results from its downward spanwise camber from the wing root towards the tip. Only a handful of studies in the past have focused on the possible efficiency gains from this particular wing design. In this section, we mention a few notable examples.

A numerical aerodynamic optimization study using both medium- and high-fidelity tools from NASA [2] considered a large degree of geometric freedom in terms of dihedral across the span using a fourth-order polynomial to allow for a continuously varying spanwise camber. The optimal shape was found to be a drooped wing with the wingtips lowered towards the ground continuously for a Boeing 767 class commercial airplane. The authors attributed the aerodynamic benefit of the drooped wing (a 5.3% reduction in induced drag in comparison to the baseline planar configuration) to its ability to move the core of the tip vortex away from the wing.

NASA had experimentally investigated the drooped wing concept under the name of Hyper-Elliptic Cambered Span (HECS) as early as 2006 [3]. This investigation was inspired by the way a seagull shapes the spanwise camber of its wings in gliding flight. The authors argued that since seagulls would naturally choose

the most efficient spanwise camber, it is possible that the drooped wing is able to provide higher efficiency than if the wings were fully extended (leading to a higher span). In other words, the drooped wing may be able to provide better aerodynamic performance than the fully extended wings with a higher span. The experimental results of this investigation eventually revealed that the drooped wing is the most beneficial configuration in comparison to planar and wingletted wings of the same projected span. It was shown to improve the maximum lift-to-drag ratio by more than 9% given the same projected span.

Another notable numerical optimization study on the seagull drooped wings [4] focused on whether the drooped wing configuration might be an aerodynamic optimum or if it occurs due to the gull's anatomical constraints. In other words, the authors were interested to see if the gulls voluntarily morph into this particular configuration rather than having been forced into it by structural motion constraints. The results of this numerical optimization study revealed that of all the configurations that a gull is able to choose from for gliding flight as dictated by its anatomical constraints, the drooped wing is the most optimal configuration from the standpoint of maximum lift-to-drag ratio. Nevertheless, this does not mean that the potential benefits of the drooped wing for gulls will be applicable to commercial aircraft.

The main objective of the present paper is to quantify the possible performance benefits from the drooped wing configuration for commercial aircraft flying at transonic speed by comparing the drooped wing to a similarly optimized planar wing. Our investigation will hopefully serve as a next step towards assessing the design trade-offs associated with the drooped wing. The analysis in the present work uses the Euler equations to model the flow along with a post-optimality viscous drag estimate based on the surface area. For the baseline Boeing 737-900 aircraft with a planar wing, we use the Vehicle Sketch Pad modeling tool developed at Cal Poly [5] to estimate that the viscous drag at cruise is equal to 200 drag counts. The larger viscous drag for the drooped wings is taken into account based on the increase in the wetted surface area relative to the baseline case [6]. This is sufficient for studying the main trends involved in the design of drooped wings. At the end of each optimization, the post-optimality viscous drag estimate will ensure that any increase in the wetted surface area is taken into account in calculating the total drag of a drooped wing. This approach does not capture the effects of viscosity on the optimal design during optimization. However, as the chord length is held fixed during the optimizations, the optimizer cannot alter the chord Reynolds number. Thus, it is not necessary to model the flow based on the RANS equations for the purpose of the current study.

The test cases presented in this paper involve giving a large amount of geometric freedom to the optimizer in order to produce nonplanar wings starting from an initially planar wing. It is important to note that this type of optimization by nature is unable to account for all the relevant operational constraints that must be taken into account. For example, the drooped wing configuration may violate the current airport

requirements in terms of wingtip vertical clearance. However, it is still important to quantify the possible efficiency gains provided by this particular design. This will help to determine whether it is worthwhile to consider, for example, high-wing aircraft in order to enable a drooped wing. The present paper does not address the possible feasibility and manufacturing challenges associated with novel designs because we believe it is first important to determine the potential performance gain.

In this paper, we size the structures based on the von Mises failure criterion at a $2.5g$ load condition [7, 8, 9, 10]. We do not consider other structural constraints such as buckling and flutter. These are potentially important considerations in this context and should be taken into account in future studies. Furthermore, we do not consider additional maneuver and gust load cases in sizing the structures. However, this does not adversely affect our main conclusions because our approach leads to similar structural component thickness distributions to those obtained from studies that include more load conditions [11, 12]. Furthermore, active maneuver and gust load alleviation systems could potentially reduce the need to include many critical structural load cases [13]. It is important to note that our objective in the present work is to study the main trends, not to perform detailed wing design. The present structural sizing strategy is sufficient for this purpose.

The design implications of the drooped wing concept for today's modern commercial aircraft are largely unknown [4]. One reason for the lack of attention to this particular configuration in the literature may be that there are uncertainties with regard to the operational and manufacturing challenges that such a configuration may introduce to the design process of an aircraft. Nonetheless, it is important to quantify the possible performance gains from this concept as part of the effort to meet the fuel efficiency gains demanded by the climate change challenge. Once these are understood, the trade-off between performance and cost can be evaluated.

II. Methodology

The aerostructural optimization code used in the present study consists of six main components: 1) a multiblock Newton-Krylov-Schur flow solver [14, 15], 2) a finite-element solver for the analysis and optimization of the structure [16], 3) a mesh movement technique based on the linear elasticity equations for moving the aerodynamic grid that is integrated with the geometry parameterization [17], 4) a surface-based free-form deformation technique for moving the structures mesh [18], 5) a B-spline parameterization method for geometry control [17], and 6) the gradient-based optimizer SNOPT [19] with gradients calculated using the discrete-adjoint method for the coupled aerostructural system using a three-field approach. Zhang et al. [20] provide a detailed description of the framework along with comprehensive verification and validation studies. The same framework has been used to study winglets for commercial transport aircraft flying at

transonic speed [21].

III. Results and Discussion

III.A. Aerostructural Optimization Problem Definition

A planform approximating the Boeing 737-900 planform with the RAE 2822 supercritical airfoil is used as the baseline wing geometry for this study. The baseline planar geometry is optimized and provides a reference for quantifying the potential benefits of drooped wings. All of the undeflected drooped and planar configurations have the same projected span. There are two main reasons for constraining the projected span. First, we are assuming that there is an airport gate constraint that prevents any increase in the span relative to the baseline wing. Second, if the drooped wings grow in span, it will not be clear whether any aerodynamic benefit is due to the increased span or the downward spanwise camber. This is due to the fact that, based on linear aerodynamic theory, the induced drag is reduced in a quadratic fashion with any increase in wing span. The relationship between induced drag and wing span is given by $D_{\text{induced}} = L^2/(\pi b^2 q_\infty e)$, where D_{induced} is the induced drag, L is the lift, b is the span, q_∞ is the dynamic pressure, and e is the span efficiency factor [22].

The objective function for the aerostructural optimization is based on the Breguet range equation and is of the form

$$\mathcal{J} = -\frac{L}{D_{\text{inviscid}}} \log \frac{W_{\text{MTO}}}{W_{\text{MTO}} - W_{\text{fuel}}}\,, \tag{1}$$

where D_{inviscid} is the calculated drag from the flow simulation based on the Euler equations. The fuel weight W_{fuel} is estimated to be around $21,000\,\text{kg}$ based on the fuel capacity of the Boeing 737-900, and W_{MTO} is the maximum takeoff weight. The maximum takeoff weight of the aircraft is assumed to be equal to the weight of the wing plus a fixed weight of $785,000\,\text{N}$ to capture the engines, fuselage, and payload weight. The cruise lift L is constrained to be equal to W_{MTO}. The cruise condition is $M = 0.785$ at an altitude of $35,000\,\text{ft}$. We emphasize that this particular choice of objective function may not be appropriate in a practical aircraft design context. However, it is sufficient for our preliminary investigation of these nonplanar wings in the context of exploratory aerostructural optimization.

Equation 1 differs from the Breguet range formulation because it does not include the viscous drag. As a result, minimizing this objective function does not necessarily maximize range due to the possible increase in the wetted surface area and hence viscous drag. Increasing the height-to-span ratio leads to a reduction in the induced drag [23]. However, from a purely aerodynamic standpoint, this reduction in induced drag will eventually be overshadowed by the increase in the viscous drag at a certain threshold if the surface area is allowed to increase. In our aerostructural optimization studies, the height-to-span ratio of the drooped

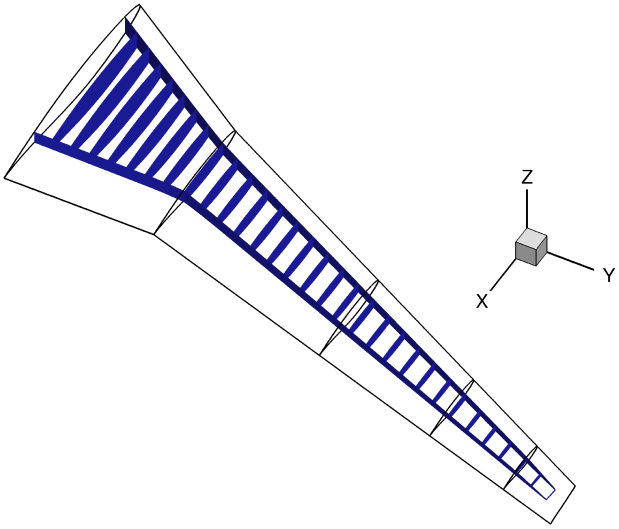

Figure 1: Primary structural layout of the ribs and spars. Skin elements are omitted for clarity.

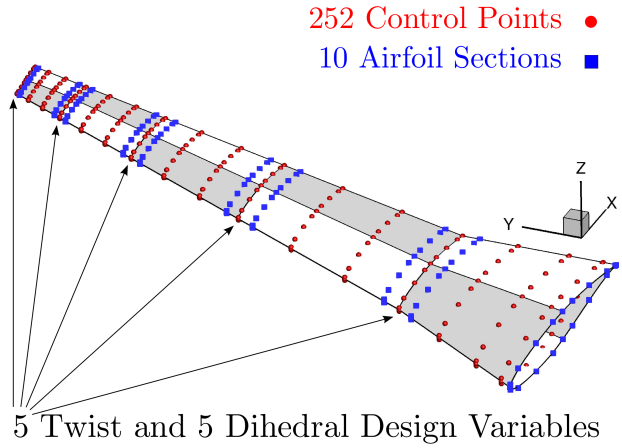

Figure 2: Geometric parameterization and design variables for the drooped wing case.

wings stops rising when the increased wing weight (and ultimately the lift required) begins to increase the lift-induced drag. This leads to a small increase in the overall surface area of the aircraft and hence the viscous drag. Furthermore, since the viscous drag is omitted for the optimization, the resulting drooped wing could be somewhat suboptimal. Therefore, our estimate of the benefits of the drooped wing is conservative in the sense that we are not overestimating its benefits.

The structural layout of the ribs and spars used is shown in Figure 1. The finite element model of the structure has approximately $30,000$ second-order shell elements. The thickness values of the structural components are allowed to vary between $5\,\text{mm}$ and $50\,\text{mm}$. Figure 2 shows the corresponding geometric parameterization and design variables. The upper and lower surfaces are each broken into 5 regions. The twist and dihedral of each region are geometric design variables. The optimizer is free to manipulate the wing section at 10 spanwise stations. The airfoil shapes are interpolated between every pair of spanwise stations

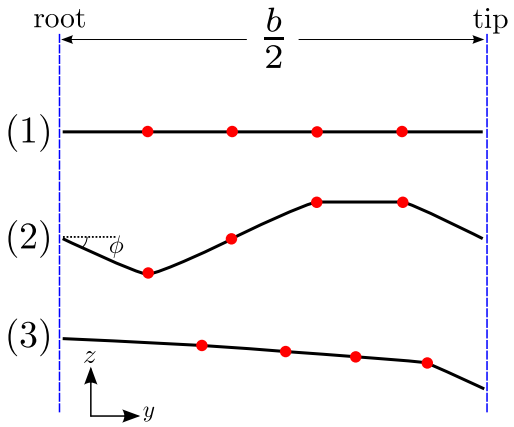

Figure 3: Three wing shapes permitted by the parameterization. Dihedral for each region can vary between $-30°$ to $+30°$.

such that curvature continuity is maintained. To further illustrate the freedom given to the optimizer to develop a nonplanar wing, Figure 3 shows simplified views of three possible wing shapes permitted by the geometric parameterization. In essence, the wings are made of five straight wing segments joined with curved junctions to maintain curvature continuity. In all cases, the projected span, leading edge sweep angle, and chord length remain constant.

Table 1 lists the constraints for each optimization test case considered in this study. There are two lift constraints; one corresponds to the cruise load condition, the other to a $2.5g$ load condition. The cruise condition is $M = 0.785$ at an altitude of $35,000\,\text{ft}$, while the $2.5g$ load condition is $M = 0.798$ at an altitude of $12,000\,\text{ft}$. The $2.5g$ load condition is based on a symmetric pull-up maneuver determined from the boundaries of the maneuvering envelope ($V - n$ diagram) for the baseline aircraft [24]. Since the weight of the wing is a function of the structural thickness values, it changes over the course of the optimization. The weight of the wing is calculated by multiplying the weight obtained from the finite-element model by a factor of 1.5 to account for the weight of the load-bearing members that are not included in the structural finite-element model of the wing, such as stringers and spar caps [25].

In practical wing design, the structures are sized based on many critical structural load conditions in order to ensure the structural integrity of the wing. The structural sizing has a profound effect on the aerodynamic performance of the wing. By considering a single $2.5g$ load condition, we aim to capture some of the effects of structural sizing on the trade-off between drag and weight [26, 10]. This means that we must constrain the calculated stresses on the structures at the $2.5g$ load condition to prevent structural failure. Three Kreisselmeier-Steinhauser (KS) constraints are used at the maneuver condition: one for the ribs and spars, one for the top skin, and one for the bottom skin. These will ensure that none of the $30,473$ finite elements in the structural model exceed the yield stress. Based on prior experimentation, we use a KS aggregation parameter of 30 for these KS constraints to strike a balance between the smoothness and

Table 1: Nonlinear constraints used for optimization in all cases

Constraint	Description
Cruise	$L - W_{\text{MTO}} = 0.0$
Maneuver	$L - 2.5W_{\text{MTO}} = 0.0$
Top Skin	$KS \leq 1.0$
Bottom Skin	$KS \leq 1.0$
Rib/Spar	$KS \leq 1.0$
Wing Span	$b = 103\,\text{ft}$
Total	6

Table 2: Optimization design variables for all cases

Design Variable	Quantity
Twist Angle	5
Dihedral Angle	5
Section Shape	140
Angle of Attack	2
Skin Thickness	60
Spar Thickness	60
Rib Thickness	30
Total	302

conservatism of the aggregated constraints [27, 20]. We use a material based on 7075 Aluminum with a Poisson's ratio $\nu = 0.33$ and Young's modulus $E = 70\,\text{GPa}$. The yield stress is $\sigma_{YS} = 434\,\text{MPa}$, and a safety factor of 2.0 is applied. In practical design of aircraft, a safety factor of 1.5 is often applied to this specific load condition. However, since we are only considering a single structural load case, it is appropriate to apply a higher safety factor in order to better capture the correct trends in structural sizing of the wing.

Table 2 provides a list of the design variables used in each case. These cases have a total of 302 design variables that control the angle of attack, geometric shape, and structural thickness distribution of the wing. Note that since chord length is not a design variable, the projected area of the wing remains unchanged. There are two angle of attack design variables: one for cruise, the other for the $2.5g$ load condition.

The optimization is initiated with an initially planar geometry. Due to the broad range of geometric freedom given to the optimizer, the drooped wing cases are particularly challenging in terms of optimization convergence. To mitigate some of these challenges, we first perform the optimizations on a coarse fluid mesh with $140,000$ nodes. Once the merit function plateaus, the optimization is continued on a finer mesh with $650,000$ nodes.

III.B. Drooped Wing Optimization Results

Figures 4 and 5 show the optimization convergence history for the drooped wing case. Feasibility is the highest nonlinear constraint violation, and optimality is a measure of the Lagrangian gradient. For a well-defined optimum, both measures should be reduced in magnitude as much as possible. After approximately 200 design iterations on the coarse grid, the merit function plateaus and the optimization is continued on the finer grid. The dashed line marks the beginning of the optimization on the finer grid. These figures indicate that the optimization reached an acceptable level of convergence. Similar convergence trends exist for the other optimization cases in this section as well.

Figure 6 shows the geometric evolution of the design during optimization. It is evident that the optimizer

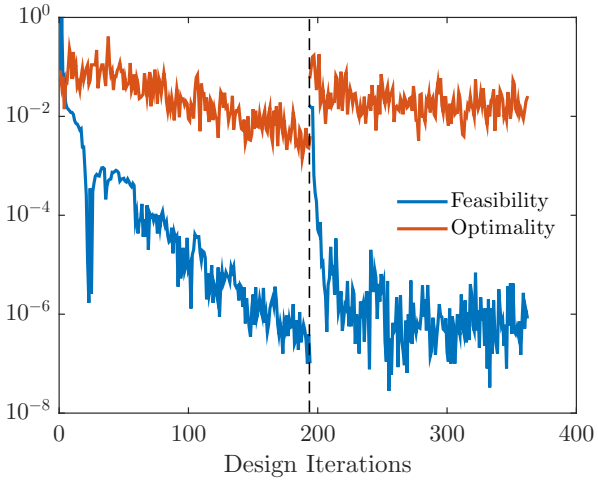

Figure 4: Convergence of optimality and feasibility conditions for the drooped wing optimization case.

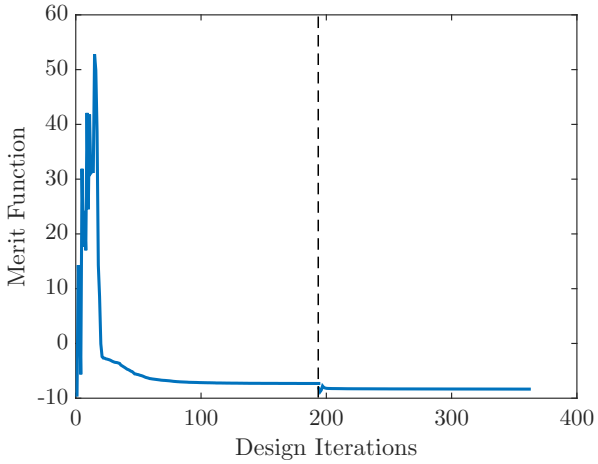

Figure 5: Merit function convergence behavior for the drooped wing optimization case.

Table 3: Optimization results for the drooped wing concept

Parameter	Planar (Straight Edges)	Drooped (Straight Edges)	Drooped (Curved Edges)	Planar (Curved Edges)
C_L	0.624	0.632	0.612	0.599
D (Counts)	410	402	384	380
L/D	15.2	15.7	15.9	15.8
W ($\times 10^5$ N)	1.32	1.37	1.30	1.28
b^* (m)	32.27	32.80	32.89	32.27
S_{wetted} (m^2)	211.8	218.4	222.5	217.1
R	3.92	4.02	4.12	4.08
ΔR	0.0%	2.6%	4.9%	4.0%

has the freedom to analyze highly nonplanar wings over the course of the optimization. Figure 6 also shows that the optimizer eventually converges to a drooped wing. This confirms that our aerostructural analysis and optimization methodology is able to recover a drooped wing concept starting from an initially planar wing.

Table 3 compares the range parameter of the optimized planar and drooped wings. The range parameter is given by $R = (L/D)\log(W_i/W_f)$, where L is the lift, D is the total drag including the viscous drag estimate based on the wetted surface area, W_i is the initial weight, and W_f is the initial weight discounted by the fuel weight. The relative differences in range are indicated by ΔR. The deflected span and surface area of the wing are denoted by b^* and S_{wetted}, respectively. The results show that the drooped wing is 2.6% more efficient than a similarly optimized planar wing of the same projected span. Figure 7 sheds some light on the reason for the efficiency improvement of the drooped wing. As Lazos and Visser [3] and Nguyen et al. [2] point out, the drooped wing moves the core of the tip vortex further away from the wing in comparison to the planar counterpart. However, our results include the additional effect of increased span at the deflected

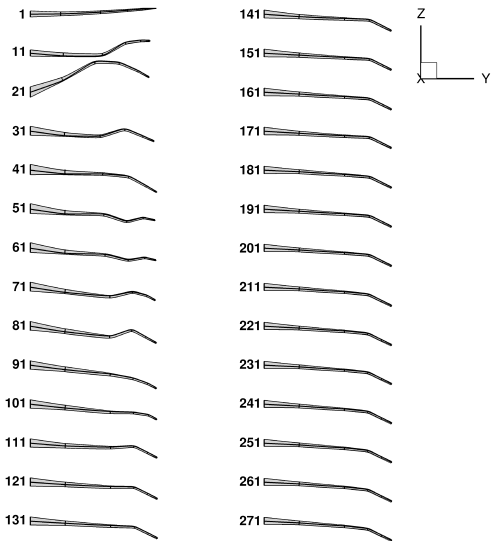

Figure 6: The geometric evolution of the drooped wing over the course of optimization.

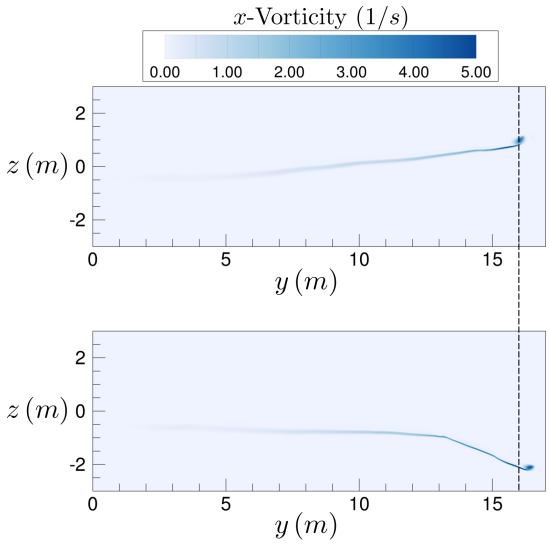

Figure 7: Contours of x-vorticity behind the trailing edge for the planar (top) and drooped (bottom) wings.

state under the aerodynamic loads. This pushes the tip vortex even further away from the wing and leads to a higher range parameter. It is interesting to note that this efficiency improvement exceeds that of the best winglet shown in Khosravi and Zingg [21].

III.C. Drooped Wing with Curved Leading and Trailing Edges

The drooped wing concepts presented by NASA [3, 2] have curved leading and trailing edges. We initially did not allow the optimizer to deviate from straight leading and trailing edges, as such wings are easier to manufacture, and this isolates the effect of the droop. We next increase the amount of geometric freedom such that the optimizer can manipulate the shape of the leading and trailing edges of the wing. Figure 8 demonstrates this additional freedom. The streamwise location of the root and tip of the wing as well as the chord length remain fixed in space. In this case, there is an additional geometric constraint to keep the projected area unchanged. This is done because the required projected area of the wing is strongly dependent on the takeoff performance requirements of the aircraft, which we do not include in our problem formulation. For the purpose of this case, we initiate the optimization using the optimal drooped wing that resulted from the previous case.

Figure 9 shows the pressure coefficient contours from a fine aerodynamic mesh with approximately 37 million nodes for the optimized drooped wing with curved leading and trailing edges. The optimizer has taken advantage of the additional geometric freedom in order to further improve the initial drooped wing design. The fine-mesh analysis indicates that this drooped wing concept with curved edges provides a 4.9% range improvement in comparison to an optimized planar wing of the same span with straight leading and

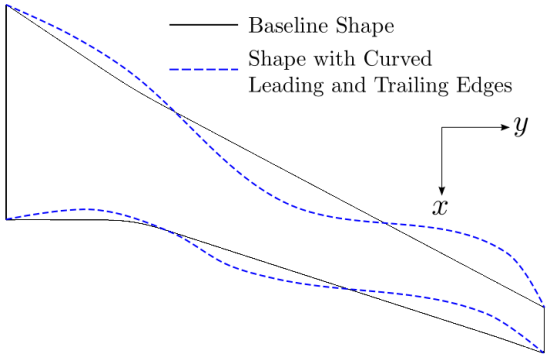

Figure 8: The additional freedom given to the optimizer to create curved leading and trailing edges.

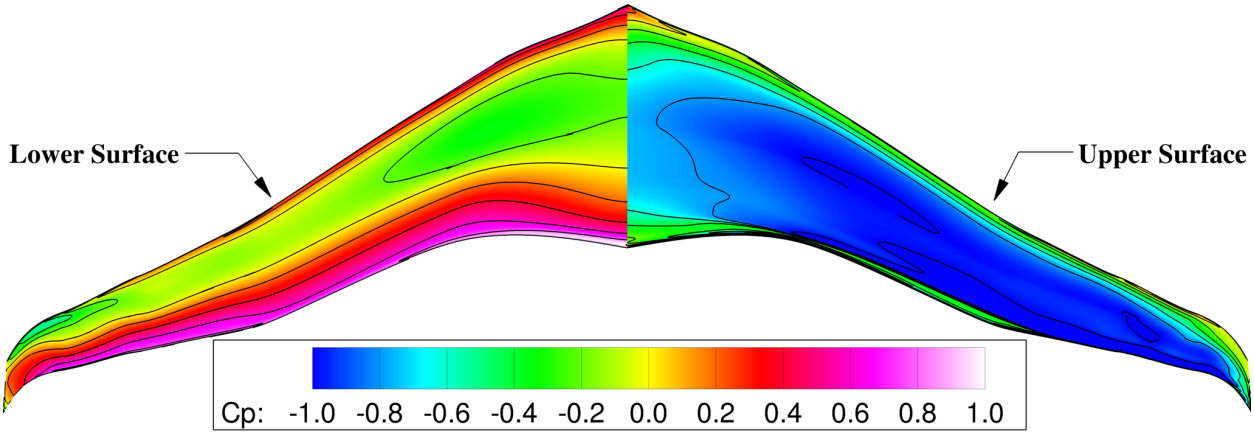

Figure 9: C_p contours from the fine mesh for the optimized drooped wing with curved leading and trailing edges.

trailing edges, as shown in Table 3.

In order to distinguish between the effect of the droop and that of the curved leading and trailing edges, a planar wing is optimized with curved leading and trailing edges permitted. The problem formulation is identical except the geometric freedom to create a nonplanar wing is removed. Figure 10 shows the initial and optimized designs that result from this optimization. As shown in Table 3, the planar wing with curved leading and trailing edges improves the objective function by 4% on the fine mesh relative to the optimal baseline planar wing with straight edges.

The optimized planar wing with curved leading and trailing edges has a lower wing weight in comparison to the optimal planar wing with linear leading and trailing edges, as shown in Table 3. Evidence for this reduction in weight can be seen in the optimal thickness distributions for the two wings. Figure 11 shows the optimal thickness values of the top and bottom skins for both designs. The additional geometric freedom has allowed the optimizer to add curvature to the main spars around the wing crank. This lowers the stress concentration by creating a fillet near the planform break and reduces the weight of the wing [28]. Although the structural topology is fixed in the present study, the aerostructural optimizer is still able to curve the spars by making changes to the leading and trailing edges of the wing. The reduction in weight leads directly

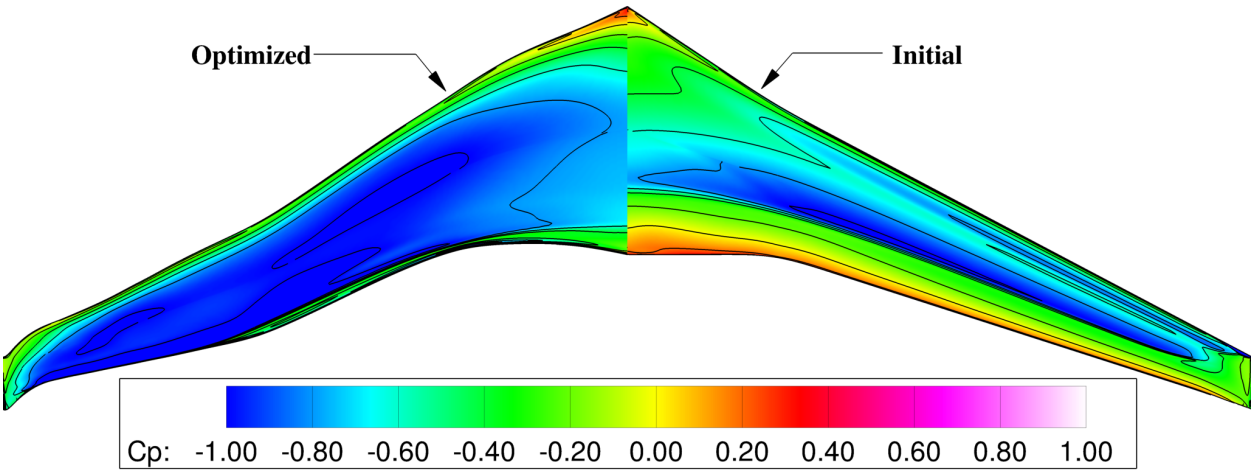

Figure 10: Initial and optimized planar configurations when the optimizer is free to create curved leading and trailing edges.

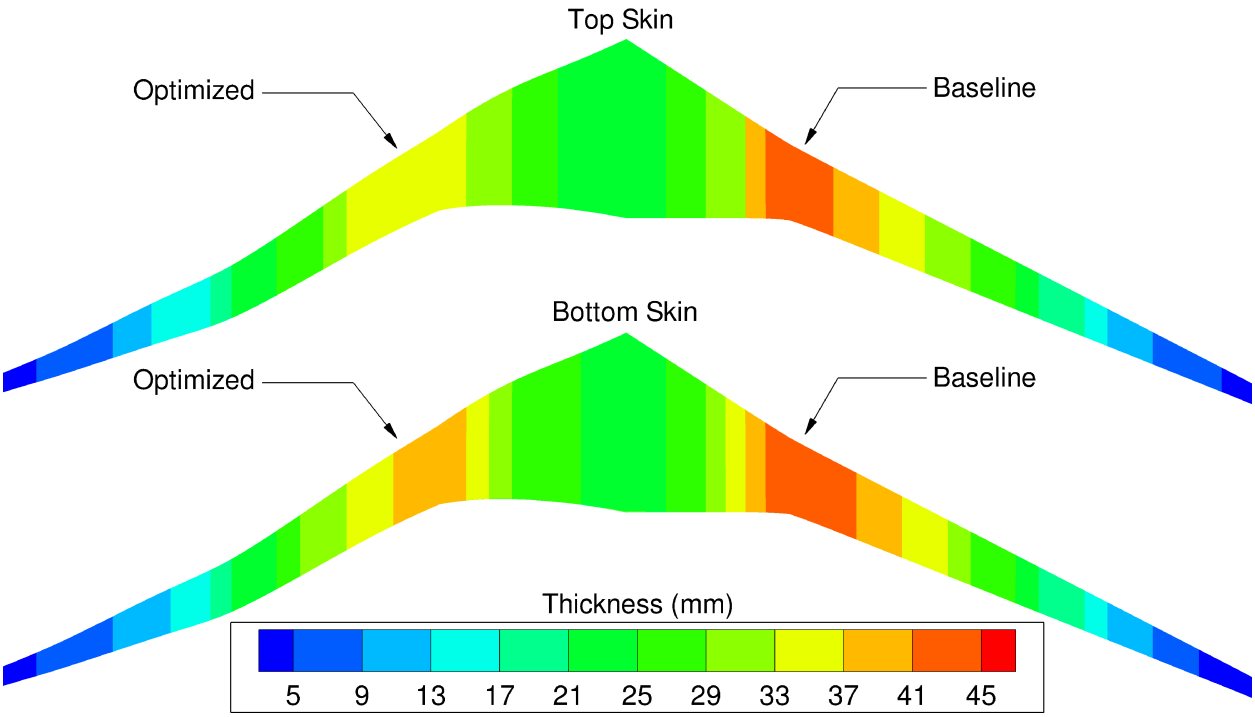

Figure 11: Optimal structural thickness distributions for the baseline and the planar wing with curved leading and trailing edges.

to improved range and also indirectly, as a lower weight leads to a lower induced drag.

The overall sweep angle of the geometry remains unchanged due to the fact that the physical locations of the wing root and tip are fixed. Having the ability to create curved leading and trailing edges allows the optimizer to vary the wing sweep locally along the span and reduce the wave drag well below its value for the optimized wing with straight edges. This may explain why the optimizer adds curvature to the wing away from the planform break. In order to examine this effect, Figures 12 and 13 show contours of normalized

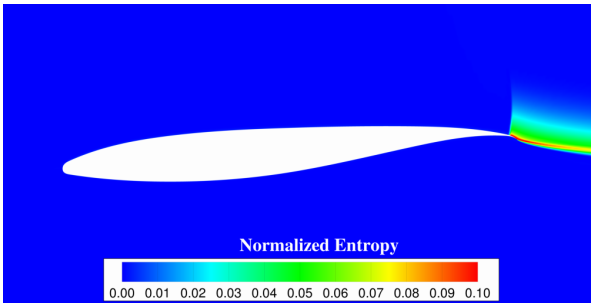

Figure 12: Normalized entropy contours in cruise at 60% half-span for the optimized planar wing with straight edges.

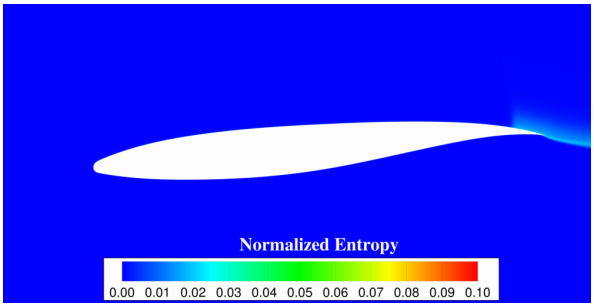

Figure 13: Normalized entropy contours in cruise at 60% half-span for the optimized planar wing with curved edges.

entropy taken at 60% of the half-span for the baseline design and the planar wing with curved leading and trailing edges, respectively. The weak shock near the trailing edge of the baseline wing, as evidenced by the discontinuity in entropy, is diminished on the wing with curved edges. As a result, some of the drag reduction provided by this design can be attributed to its ability to reduce the wave drag.

We can use purely aerodynamic shape optimization based on the Euler equations to confirm that the planar wing with curved leading and trailing edges reduces the wave drag by locally varying wing sweep along the span. We perform a lift-constrained drag minimization with $C_L = 0.62$ at Mach 0.785 using the same geometric parameterization as the previous case. The inviscid lift-to-drag ratio of the wing with curved edges is approximately 6.7% higher than the planar wing with straight edges. However, we still need to address the possibility that some of this drag reduction may be due to induced drag savings from a nonplanar wake.

In order to examine the possibility that a wing with curved leading and trailing edges can reduce the induced drag by producing a nonplanar wake, we consider a purely aerodynamic shape optimization case at a cruise Mach number of 0.50. Since the flow is inviscid and the low Mach number eliminates wave drag as a potential source of drag, only induced drag remains. We conduct a lift-constrained drag minimization with $C_L = 0.62$ using the same geometric parameterization as before. The inviscid lift-to-drag ratio of the wing with curved leading and trailing edges is only 0.5% higher than that of the baseline wing, indicating that curved leading and trailing edges do not significantly enhance the induced drag performance of swept-back wings, which already produce a nonplanar wake at a nonzero angle of attack [29, 30].

Our preliminary investigation of the drooped wing concept has shown that it can improve the range of the baseline aircraft. However, this nonplanar geometry will have important practical implications on the design of the aircraft that are beyond the scope of the present study. The negative dihedral of the drooped wing may necessitate a high-wing configuration in order to maintain a reasonable lateral static stability margin [31]. A high-wing configuration may also be required to accommodate wingtip vertical clearance requirements. However, this may not be a significant disadvantage, as a high-wing configuration may be aerodynamically more efficient than today's modern low-wing aircraft [32].

III.D. Multimodality of the Drooped Wing

Given that a gradient-based optimization algorithm has been used, it is important to consider the possibility that the optimum found is a local optimum rather than the global optimum. Past research efforts have found that, in the context of purely aerodynamic shape optimization based on the Euler equations, wing design problems with significant amount of geometric freedom can be somewhat multimodal [33]. Furthermore, the number of local optima increases with increasing geometric freedom. This presents a well-known and significant challenge for gradient-based optimization methodologies that do not have a mechanism to ensure convergence to the global optimum, especially in cases where the number of design variables is on the order of hundreds.

A formal investigation of multimodality involves generating many samples to serve as initial designs in order to ensure that all regions of the design space are sufficiently represented. Sophisticated sampling strategies, including Latin hypercube and Sobol sequences, already exist for efficient exploration of the design space. However, using these strategies requires optimizing many different initial geometries and assessing the shape and performance of each optimized sample. Such a study is outside the scope of the present investigation and would require an excessive amount of computational resources due to the fact that performing high-fidelity aerostructural optimization is computationally expensive. As a result, we limit our preliminary investigation to using a few randomly generated initial geometries using the same parameterization presented in Section III.A. The randomly perturbed design variables include the five dihedral and twist angle values at the specified spanwise stations. The problem formulation in terms of objective function and nonlinear constraints is the same as before.

Figure 14 shows the six initial geometries used for the purpose of this investigation. Although the number of initial samples is not large enough to explore the design space thoroughly, it still represents a significant deviation from using a single initial design. Figure 15 shows all final geometries. It is clear that the optimizations lead to similar drooped wing concepts regardless of the initial geometry used. Table 4 shows the final objective function values of all designs. Differences in the objective function are indicated by $\Delta\mathcal{J}$. The performance of all six optimal designs is also similar. Although they do not provide definitive proof, these results suggest that the optimization problem presented here is most likely not multimodal.

IV. Conclusions

This paper has presented an investigation of the potential performance benefits of drooped wings by comparing a drooped wing optimized for maximum range through aerostructural optimization with a similarly optimized planar wing. Both straight and curved leading and trailing edges have been considered. The most important conclusions from the drooped wing investigation are listed below.

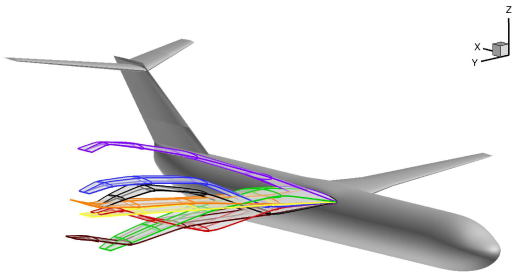

Figure 14: Randomly generated initial geometries.

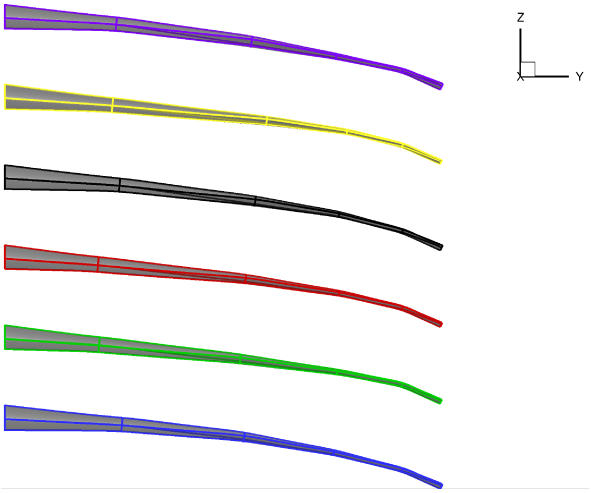

Figure 15: Final optimized designs from the initial geometries shown in Figure 14.

Table 4: The final objective function comparison for all of the six optimized designs evaluated

Parameter	Design 1	Design 2	Design 3	Design 4	Design 5	Design 6
$\mathcal{J}$	-8.73	-8.76	-8.78	-8.77	-8.75	-8.75
$\Delta\mathcal{J}$	0.0%	0.3%	0.6%	0.5%	0.2%	0.2%

- The drooped wing with straight leading and trailing edges can improve the range by 2.6% in comparison to an optimal planar wing of the same span. This configuration moves the tip vortex further away from the wing in the spanwise direction compared to the planar wing.

- Commercial aircraft wings may benefit from allowing the leading and trailing edges to be curved. Specifically, removing the wing crank may reduce the wing weight considerably. Heavier wings require more lift and as a result lead to higher lift-induced drag. Our results show an overall 4% range improvement for a planar wing with curved leading and trailing edges compared to one with straight leading and trailing edges. However, there are practical reasons and constraints for having a crank and straight leading and trailing edges. Nevertheless, our purpose in exploratory optimization studies of this nature is to quantify the relative efficiency improvement that is possible by relaxing such constraints.

- The drooped wing with curved leading and trailing edges can improve the range by 4.9% relative to a planar wing with straight leading and trailing edges of the same projected span.

- The drooped wing leads to a higher range than wingletted wings [21] with the same undeflected projected span. However, it is important to acknowledge that it is easier to manufacture wingletted wings than drooped wings.

Acknowledgments

The authors gratefully acknowledge the financial support provided by the Ontario Graduate Scholarship program, the National Science and Engineering Research Council, and the University of Toronto. Computations were performed on the GPC supercomputer at the SciNet HPC Consortium. SciNet is funded by the Canada Foundation for Innovation under the auspices of Compute Canada, the Government of Ontario, Ontario Research Fund - Research Excellence, and the University of Toronto. Furthermore, the authors acknowledge Prof. Joaquim R. R. A. Martins of the University of Michigan, Ann Arbor for sharing his framework for the purpose of constructing our methodology.

References

[1] "Global Market Forecast 2015," Tech. rep., Airbus S.A.S., August 2015.

[2] Nguyen, N., Trinh, K., Reynolds, K., Kless, J., Aftosmis, M., Urnes, J., and Ippolito, C., "Elastically Shaped Wing Optimization and Aircraft Concept for Improved Cruise Efficiency," *51st AIAA Aerospace Sciences Meeting including the New Horizons Forum and Aerospace Exposition*, No. AIAA 2013-0141, Grapevine (Dallas/Ft. Worth Region), Texas, January 2013. doi:10.2514/6.2013-141.

[3] Lazos, B. and Visser, K., "Aerodynamic Comparison of Hyper-Elliptic Cambered Span (HECS) Wings with Conventional Configurations," *24th AIAA Applied Aerodynamics Conference*, No. AIAA 2006-3469, San Francisco, California, June 2006. doi:10.2514/6.2006-3469.

[4] Andrews, S. A., Perez, R. E., and Allan, W. D. E., "Aerodynamic implications of gull's drooped wing-tips," *Bioinspiration and Biomimetics*, Vol. 8, No. 4, 2013, pp. 046003. doi:10.1088/1748-3182/8/4/046003.

[5] Fredericks, W., Costa, K. A. G., Deshpande, N., Moore, M., Miguel, E. S., and Snyder, A., "Aircraft Conceptual Design Using Vehicle Sketch Pad," *48th AIAA Aerospace Sciences Meeting Including the New Horizons Forum and Aerospace Exposition*, No. AIAA 2010-658, Orlando, Florida, January 2010. doi:10.2514/6.2010-658.

[6] Gur, O., Mason, W. H., and Schetz, J. A., "Full-Configuration Drag Estimation," *Journal of Aircraft*, Vol. 47, No. 4, 2010, pp. 1356–1367. doi:10.2514/1.47557.

[7] Ciampa, P. D. and Nagel, B., "Aerostructural Interaction in a Collaborative MDO Environment," *International Conference of Computational Methods in Sciences and Engineering 2014 (ICCMSE)*, Athens, Greece, April 2014. doi:10.1063/1.4897753.

[8] Viti, A., Druot, T., and Dumont, A., "Aero-structural approach coupled with direct operative cost optimization for new aircraft concept in preliminary design," *17th AIAA/ISSMO Multidisciplinary Analysis and Optimization Conference*, No. AIAA 2016-3512, Washington, District of Columbia, June 2016. doi:10.2514/6.2016-3512.

[9] Kenway, G. K. W., Kennedy, G. J., and Martins, J. R. R. A., "A CAD-Free Approach to High-Fidelity Aerostructural Optimization," *Proceedings of the 13th AIAA/ISSMO Multidisciplinary Analysis Optimization Conference*, No. AIAA 2010-9231, Fort Worth,Texas, September 2010. doi:10.2514/6.2010-9231.

[10] Kennedy, G. J. and Martins, J. R. R. A., "Parallel Solution Methods for Aerostructural Analysis and Design Optimization," *13th AIAA/ISSMO Multidisciplinary Analysis Optimization Conference*, No. AIAA-2010-9308, Fort Worth, Texas, September 2010. doi:10.2514/6.2010-9308.

[11] Kennedy, G. J. and Martins, J. R. R. A., "A Comparison of Metallic and Composite Aircraft Wings Using Aerostructural Design Optimization," *14th AIAA/ISSMO Multidisciplinary Analysis and Optimization Conference*, No. AIAA 2012-5475, Indianapolis, IN, September 2012. doi:10.2514/6.2012-5475.

[12] Kenway, G. K. W., Kennedy, G. J., and Martins, J. R. R. A., "Aerostructural optimization of the Common Research Model configuration," *15th AIAA/ISSMO Multidisciplinary Analysis and Optimization Conference*, No. 2014-3274, Atlanta, Georgia, June 2014. doi:10.2514/6.2014-3274.

[13] Fonte, F., Ricci, S., and Mantegazza, P., "Gust Load Alleviation for a Regional Aircraft Through a Static Output Feedback," *Journal of Aircraft*, Vol. 52, No. 5, 2015, pp. 1559–1574. doi:10.2514/1.C032995.

[14] Hicken, J. E. and Zingg, D. W., "Parallel Newton-Krylov Solver for the Euler Equations Discretized Using Simultaneous-Approximation Terms," *AIAA Journal*, Vol. 46, No. 11, 2008, pp. 2773–2786. doi:10.2514/1.34810.

[15] Osusky, M. and Zingg, D. W., "Parallel Newton-Krylov-Schur Solver for the Navier-Stokes Equations Discretized Using Summation-By-Parts Operators," *AIAA Journal*, Vol. 51, No. 12, 2013, pp. 2833–2851. doi:10.2514/1.J052487.

[16] Kennedy, G. J. and Martins, J. R. R. A., "A parallel finite-element framework for large-scale gradient-based design optimization of high-performance structures," *Finite Elements in Analysis and Design*, Vol. 87, September 2014, pp. 56–73. doi:10.1016/j.finel.2014.04.011.

[17] Hicken, J. E. and Zingg, D. W., "Aerodynamic Optimization Algorithm with Integrated Geometry Parameterization and Mesh Movement," *AIAA Journal*, Vol. 48, No. 2, 2010, pp. 400–413. doi:10.2514/1.44033.

[18] Zhang, Z. J., Khosravi, S., and Zingg, D. W., "High-Fidelity Aerostructural Optimization with Integrated Geometry Parameterization and Mesh Movement," *56th AIAA/ASCE/AHS/ASC Structures, Structural Dynamics, and Materials Conference*, No. AIAA 2015-1132, Kissimmee, Florida, January 2015. doi:10.2514/6.2015-1132.

[19] Gill, P. E., Murray, W., Michael, and Saunders, M. A., "SNOPT: An SQP Algorithm For Large-Scale Constrained Optimization," *SIAM Journal on Optimization*, Vol. 12, 1997, pp. 979–1006. doi:10.1137/S0036144504446096.

[20] Zhang, Z. J., Khosravi, S., and Zingg, D. W., "High-Fidelity Aerostructural Optimization with Integrated Geometry Parameterization and Mesh Movement," *Structural and Multidisciplinary Optimization*, Vol. 55, 2016, pp. 1217–1235. doi:10.1007/s00158-016-1562-7.

[21] Khosravi, S. and Zingg, D. W., "Aerostructural Perspective on Winglets," *Journal of Aircraft*, Vol. 3, No. 54, May 2017, pp. 1121–1138. doi:10.2514/1.C033914.

[22] Anderson, J. D., *Fundamentals of Aerodynamics*, McGraw-Hill, 1221 Avenue of the Americas, New York, NY 10020, United States of America, 4th ed., 2007.

[23] Kroo, I., "Drag Due to Lift: Concepts for Prediction and Reduction," *Annual Review of Fluid Mechanics*, Vol. 33, No. 1, 2001, pp. 587–617. doi:10.1146/annurev.fluid.33.1.587.

[24] Raymer, D. P., *Aircraft Design : A Conceptual Approach*, American Institute of Aeronautics and Astronautics, 12700 Sunrise Valley Drive, Suite 200 Reston, VA 20191-5807, United States of America, 5th ed., 2012. doi:10.2514/4.869112.

[25] Kennedy, G. and Martins, J., "A parallel aerostructural optimization framework for aircraft design studies," *Structural and Multidisciplinary Optimization*, Vol. 50, No. 6, 2014, pp. 1079–1101. doi:10.1007/s00158-014-1108-9.

[26] Jansen, P., Perez, R. E., and Martins, J. R. R. A., "Aerostructural Optimization of Nonplanar Lifting Surfaces," *Journal of Aircraft*, Vol. 47, No. 5, 2010, pp. 1491–1503. doi:10.2514/1.44727.

[27] Kennedy, G. J. and Hicken, J. E., "Improved constraint-aggregation methods," *Computer Methods in Applied Mechanics and Engineering*, Vol. 289, 2015, pp. 332 – 354. doi:10.1016/j.cma.2015.02.017.

[28] Gregg, R. D. and McDowell, D. L., "Blended Leading and Trailing Edge Wing Planform," June 2005, U.S. Patent 10/717,366.

[29] van Dam, C. P., "Induced-Drag Characteristics of Crescent-Moon-Shaped Wings," *Journal of Aircraft*, Vol. 24, No. 2, 1987, pp. 115–119. doi:10.2514/3.45427.

[30] van Dam, C. P., "Aerodynamic Characteristics of Crescent and Elliptic Wings at High Angles of Attack," *Journal of Aircraft*, Vol. 28, No. 4, 1991, pp. 253–260. doi:10.2514/3.46020.

[31] Anderson, J. D., *Aircraft Performance and Design*, McGraw-Hill, 1221 Avenue of the Americas, New York, NY 10020, United States of America, 1st ed., 1998.

[32] Hashimoto, A., Jeong, S., and Obayashi, S., "Aerodynamic Optimization of Near-future High-wing Aircraft," *Transactions of the Japan Society for Aeronautical and Space Sciences*, Vol. 58, No. 2, 2015, pp. 73–82. doi:10.2322/tjsass.58.73.

[33] Chernukhin, O. and Zingg, D. W., "Multimodality and Global Optimization in Aerodynamic Design," *AIAA Journal*, Vol. 51, No. 6, 2013, pp. 1342–1354. doi:10.2514/1.J051835.